

CH_x adsorption ($x=1-4$) and thermodynamic stability on the CeO₂(111) surface: A first-principles investigation

Marco Fronzi,^{1,*} Simone Piccinin,² Bernard Delley,³ Enrico Traversa,⁴ and Catherine Stampfl⁵

¹*Department of Mechanical Science and Bioengineering,*

Graduate School of Engineering Science, Osaka University, Japan

²*CNR-IOM Democritos, c/o SISSA, via Bonomea 265, I-34136 Trieste, Italy*

³*Paul-Scherrer-Institut, CH-5232 Villigen PSI, Switzerland*

⁴*Physical Sciences and Engineering Division, King Abdullah University of Science and Technology, Kingdom of Saudi Arabia*

⁵*School of Physics, The University of Sydney, Sydney, New South Wales 2006, Australia*

(Dated: September 12, 2018)

We present an *ab initio* investigation of the interaction between methane, its dehydrogenated forms and the cerium oxide surface. In particular, the stoichiometric CeO₂(111) surface and the one with oxygen vacancies are considered. We study the geometries, energetics and electronic structures of various configurations of these molecules adsorbed on the surface in vacuum, and we extend the analysis to realistic environmental conditions. A phase diagram of the adsorbate-surface system is constructed and relevant transition phases are analyzed in detail, showing the conditions where partial oxidation of methane can occur.

PACS numbers: 68.43.-h, 68.47.Gh

I. INTRODUCTION

The fuel cell technology developed in the past years has become an area of great interest, due to the high potential for the production of clean energy.^{1,2} The research in this field aims to produce more efficient materials to be used as electrodes with a high and selective catalytic activity, in order to improve the efficiency of energy production and also to reduce the operating temperature of these devices. Therefore, recently many studies have been performed in order to analyze molecule-surface interactions and surface catalytic activity of several metal oxide compounds from both an experimental and a theoretical point of view.^{3,4}

Cerium oxide has been considered a good candidate as an electrolyte material and an electrode support due to its desirable characteristic of storing oxygen, as well as its surface catalytic activity.⁵⁻⁹ Its surfaces show activity with respect to several chemical reactions, in particular for the C-H bond cracking of the methane molecule, proving that CeO_{2-x} acts as active center for methane oxidation.¹⁰ This makes it a good candidate to be used as a fuel cell anode material.^{11,12} On the other hand, methane is the main component of natural gas and there is a keen interest to understand the mechanisms of methane oxidation, used for energy production.^{13,14} Direct oxidation of methane on both metal and metal-oxide surfaces has been observed, showing a very high thermodynamic efficiency limit for complete oxidation, that can reach 92%.^{12,15,16} Indeed, experiments proved that methane shows chemical activity if exposed to an atmosphere containing oxygen and that a humid environment play an important role against methane oxidation.¹⁷⁻¹⁹ From this perspective, a systematic study of CH_x adsorption on cerium oxide surfaces under realistic catalytic conditions becomes crucial to improve the efficiency of important processes in chemical industries.

Several theoretical computational studies have been carried out to study methane dissociation on CeO₂ under vacuum conditions.^{12,20} In this paper we want to examine this system when in contact with two gas reservoirs, oxygen and water vapor, by means of *ab initio* atomistic thermodynamics, in order to reproduce realistic environmental conditions.²¹⁻²⁴

Using a computational Density Functional Theory (DFT) approach, in this work we provide a systematic analysis of CH_x adsorption on the stoichiometric, as well as the reduced, CeO₂(111) surface. We analyze the CH_x fragment adsorption energies in vacuum, and describe the adsorbate-surface bonds obtained by charge distribution in the adsorption process and the electronic structures of the adsorbate-surface system. The calculated adsorption and surface energies enable us to describe the trend of the Gibbs free energy under realistic catalytic conditions as a function of the chemical potential of the oxygen and water. The analysis results in the construction of a surface phase diagram that shows the relative thermodynamic stability of each adsorbate-surface system; also, relevant transition phases can be analyzed in detail.

II. DETAILS OF METHODOLOGY

A. DFT calculations: basis set and convergence

All calculations presented in this work are performed using the generalized gradient approximation for the exchange and correlation potential due to Perdew, Burke and Erzerhof (PBE) as implemented in the all-electron DMol³ code.²⁵⁻²⁷ The DMol³ method employs fast converging three-dimensional numerical integrations to calculate the matrix elements occurring in the Ritz variational method. The wave functions are expanded in terms of a double-numerical quality localized basis set

TABLE I: Adsorption energies of CH_4 on different adsorption sites of the $\text{CeO}_2(111)$ surface. Namely, on top of the Ce atom, O atom, surface oxygen vacancy (V_{O}) and the oxygen atom located in the second layer ($\text{O}_{2\text{nd}}$).

Config.	Adsorption energy (eV)
Ce	-0.07
O	-0.05
$\text{O}_{2\text{nd}}$	-0.06
V_{O}	0.00

with a real-space cutoff of 11 Bohr. Polarization functions and scalar-relativistic corrections are incorporated explicitly. We use (2×2) surface unit cells, and a vacuum region of $\approx 30 \text{ \AA}$, which ensures negligible interaction between periodic replicas, and an $8 \times 8 \times 1$ \mathbf{k} -point mesh, yielding 10 \mathbf{k} -points in the irreducible part of the Brillouin Zone. Further details about the use of DFT on systems containing reduced CeO_2 can be found elsewhere.^{28,29}

III. GEOMETRIES AND ENERGETICS

In this section, we analyze energetics and geometries of the interaction between the CH_x ($x=1-4$) and the $\text{CeO}_2(111)$ surface with and without surface oxygen vacancies, when the CH_x coverage is 0.25 ML under vacuum conditions. We start by considering the interaction of CH_4 with the $\text{CeO}_2(111)$ surface. Various configurations are considered for adsorption, as reported in Tab.I, where the adsorption energies are calculated as follows:

$$E_{\text{ads}} = E_{\text{sys}} - E_{\text{surf}} - E_{\text{mol}}, \quad (1)$$

where E_{surf} is the surface energy, E_{mol} the isolated molecule energy, and E_{sys} is the surface-adsorbate system.

For the considered configurations, the methane molecule shows a weak interaction with the $\text{CeO}_2(111)$ surface. In the most favorable case, it adsorbs at the cerium site, with an adsorption energy of -0.07 eV . In this configuration, shown in Fig. 1, the methane molecule adsorbs on the surface with a hydrogen atom pointing to the surface cerium atom. The distance Ce-O in this case is 2.51 \AA . In this case, the energy value of the adsorbate-surface bond is very small, showing an extremely weak interaction. This result is in line with other results in the literature, using both DFT and DFT+U approaches.²⁰ When an oxygen vacancy is created on the cerium oxide surface, interestingly, the interaction become repulsive. The morphology of the surface becomes therefore crucial for the first step in the methane oxidation reaction. To better analyze the nature of the interaction between CH_4 and the surface cerium atom, we studied the charge density difference (Q_d) induced by the

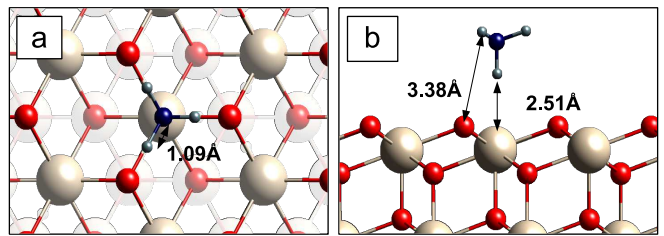


FIG. 1: (Color online) Top (a) and side (b) view of adsorption sites considered for methane on the $\text{CeO}_2(111)$. (a) and (b) show methane in the Ce configuration. Large pale (gray) and small dark (red) spheres indicate Ce and O atoms, respectively. The small dark (blue) and the very small (gray) spheres represent C and H atoms respectively. Selected interatomic distances are indicated.

adsorption of water on $\text{CeO}_2(111)$, defined as the difference between the charge density of the adsorbate system (Q_{s+a}) and the sum of the isolated molecule (Q_a) and the slab (Q_s), calculated as follows:

$$Q_d = Q_{s+a} - (Q_s + Q_a). \quad (2)$$

In this case, an extremely small charge redistribution is observed (therefore not reported here). The adsorption energy in the proximity of an oxygen vacancy shows a slightly repulsive interaction between methane molecule and surface.

In order to obtain a first insight in the analysis of the CH_4 dissociation on the $\text{CeO}_2(111)$ surface, we examine the adsorption of CH_x fragments. The CH_3 fragment adsorbs on the oxygen atom site with an adsorption energy of -2.09 eV , and the distance between carbon atom and surface oxygen is 1.40 \AA (see Tab.II). The adsorption on the cerium atom and over the oxygen in the second layer are highly unfavored and the energy indicates a repulsive interaction. When an oxygen vacancy is created on the surface, the adsorption energy decreases to -1.80 eV , indicating a less favorable interaction between molecule and reduced surface. The induced charge density of CH_3 adsorption on the $\text{CeO}_2(111)$ indicates a charge redistribution, as shown in Fig.3, which shows an evident charge transfer from the surface oxygen toward the carbon. The charge accumulation is not strongly localized, likely due to the presence of an unpaired electron of the carbon atom. However, the shared charge can be an indication of a covalent bond between the carbon atom of the fragment and the surface oxygen.

The CH_2 fragment interacts strongly with the surface, having a strong adsorption energy on both the Ce and O sites (-3.26 eV and -3.31 eV , respectively). Even when it adsorbs on an oxygen vacancy, the adsorption energy differs from the most stable configuration only by 9.3% of the energy bond (see Tab.III). The analysis of the induced charge density indicates an evident charge transfer from the surface oxygen to the carbon atom. The shared electron charge suggests the formation of a covalent bond.

TABLE II: adsorption energies (in eV) of CH_3 on the $\text{CeO}_2(111)$ surface in different configurations. Namely, on top of the O atom and the surface oxygen vacancy (V_{O}).

Config.	adsorption energy
O	-2.09
V_{O}	-1.80

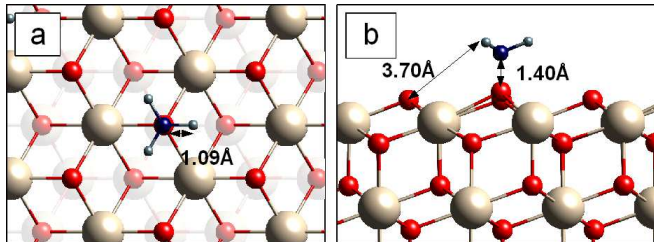


FIG. 2: (Color online) Top (a) and side (b) view of adsorption sites considered for CH_3 fragment on $\text{CeO}_2(111)$. (a) and (b) show CH_3 in the O configuration. The small dark (blue) and the very small (gray) spheres represent C and H atoms respectively. Selected inter-atomic distances are indicated.

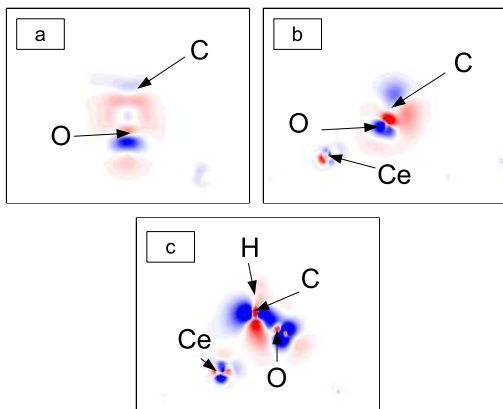


FIG. 3: (Color online) Induced charge density due to the adsorption of (a) CH_3 , (b) CH_2 and (c) CH on the $\text{CeO}_2(111)$ surface. The red areas indicate charge accumulation, while the blue areas indicate charge depletion.

TABLE III: Adsorption energies (in eV) of CH_2 on the $\text{CeO}_2(111)$ surface in different configurations. Namely, on top of the Ce atom, O atom and surface oxygen vacancy (V_{O}).

Config.	adsorption energy (eV)
Ce	-3.26
O	-3.31
V_{O}	-3.00

The last fragment analyzed in this section is CH . In this case the adsorption energy is very high when it adsorbs on both the Ce and O sites (-4.07 eV and -4.14 eV, respectively) and when an oxygen vacancy is created

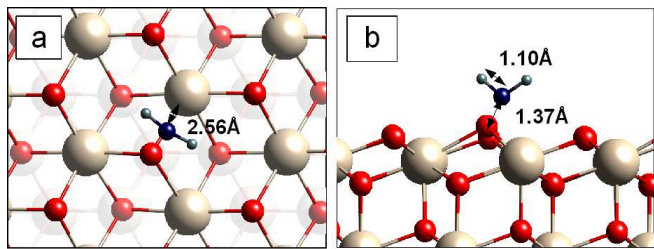


FIG. 4: (Color online) Top (a) and side (b) view of adsorption sites considered for CH_2 on the $\text{CeO}_2(111)$. (a) and (b) show CH_2 in the O configuration. Large pale (gray) and small dark (red) spheres indicate Ce and O atoms, respectively. The small dark (blue) and the very small (gray) spheres represent C and H atoms respectively. Selected inter-atomic distances are indicated.

TABLE IV: adsorption energies (in eV) of CH on the $\text{CeO}_2(111)$ surface in different configurations. Namely, on top of the Ce atom, O atom and surface oxygen vacancy (V_{O}).

Config.	adsorption energy (eV)
Ce	-4.07
O	-4.14
V_{O}	-2.96

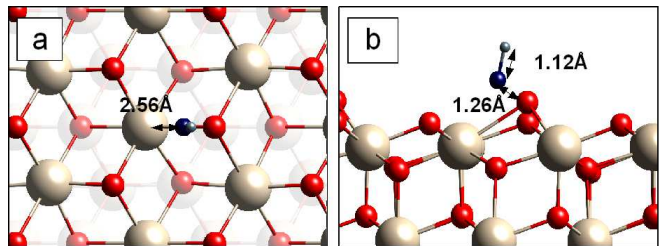


FIG. 5: (Color online) Top (a) and side (b) view of adsorption sites considered for CH fragment on $\text{CeO}_2(111)$. (a) and (b) show CH in the O configuration. Large pale (gray) and small dark (red) spheres indicate Ce and O atoms, respectively. The small dark (blue) and the very small (gray) spheres represent C and H atoms respectively. Selected inter-atomic distances are indicated.

on the surface, the interaction energy decreases to -2.96 eV, indicating a strong interaction between the oxygen vacancy and the CH fragment. The induced charge density for the adsorption on the O site of $\text{CeO}_2(111)$ indicates an evident charge transfer. Figure 3 shows a charge depletion around the surface oxygen and around the carbon atom in the plane cutting the aligned C,O Ce and H atoms. To obtain information about the bond formation, more detailed three dimensional charge distribution around the carbon atom is necessary. However, the evident charge redistribution around the cerium atom suggests a possible interaction between the carbon atom and the lower lying cerium atom.

IV. ENERGETICS AND THERMODYNAMICS

In this section we analyze the stability of the surfaces under the realistic environmental conditions of a humid atmosphere (H_2O) containing pure oxygen gas. Each adsorbate-surface system, previously considered in a vacuum space, is now analyzed when in thermodynamic equilibrium with two independent reservoirs of oxygen gas and water in its vapor phase. We take into consideration the situation where the $\text{CeO}_2(111)$ surface has one of the CH_x fragment adsorbed, and where the oxygen and water chemical potentials can hypothetically vary independently to each other within two extreme limits of poor and rich concentration. This approach allows us to calculate the energy of each surface-molecule system under every possible value of oxygen/water partial pressure. The surface free energy for each of the surface-molecule systems is calculated as follows:

$$\gamma(\{p_i\}, T) = \frac{1}{2A} \left[G - \sum N_i \mu_i(p_i, T) \right], \quad (3)$$

where G is the Gibbs free energy of the solid with surface area A (the factor $\frac{1}{2}$ is due to the presence of two identical surfaces, one on each side of the slab); $\mu(p_i, T)$ is the chemical potential of the species i that depends on pressure and temperature of the system, and N_i is number of atoms of component i of the system.

The chemical potentials, $\mu(p, T)$, of oxygen and water vapor depend on temperature and pressure according to:

$$\mu_{\text{O}}(p, T) = \frac{1}{2} \left[E_{\text{O}_2} + \tilde{\mu}_{\text{O}_2}(p^0, T) + k_B T \ln \left(\frac{p_{\text{O}_2}}{p^0} \right) \right] \quad (4)$$

$$\mu_{\text{H}_2\text{O}}(p, T) = E_{\text{H}_2\text{O}} + \tilde{\mu}_{\text{H}_2\text{O}}(p^0, T) + k_B T \ln \left(\frac{p_{\text{H}_2\text{O}}}{p^0} \right) \quad (5)$$

In Fig.6 these quantities are re-defined in order to have 0 eV as oxygen and water rich-limit conditions, and the plot is constructed as a function of $\Delta\mu_{\text{O}_2}$ and $\Delta\mu_{\text{H}_2\text{O}}$. For this specific system, the poor-limit conditions for the chemical potentials are $\Delta\mu_{\text{O}_2} > -5.01$ eV and $\Delta\mu_{\text{H}_2\text{O}} < -0.91$ eV. A more detailed description of the derivation of these quantities can be found elsewhere.²⁹

Equation 3 describes the surface free energy, γ for each of the surface-molecule systems, i.e. a function of the two variables $\Delta\mu_{\text{O}_2}$ and $\Delta\mu_{\text{H}_2\text{O}}$. For each value of $\Delta\mu_{\text{O}_2}$ and $\Delta\mu_{\text{H}_2\text{O}}$, the value of γ with lower energy is the most thermodynamically stable. Figure 6 is obtained by projecting the surface with the lowest free energy on the $\Delta\mu_{\text{O}_2} - \Delta\mu_{\text{H}_2\text{O}}$ planes so that each colored area represents the most stable surface-molecule system for given values of the chemical potential of oxygen and water. In Fig. 6, the plot can be divided in two main areas: one including the blue and the red ones where CH_4 is stable on the reduced and stoichiometric surfaces, respectively, and the rest of them where the CH_4 is not stable. In these

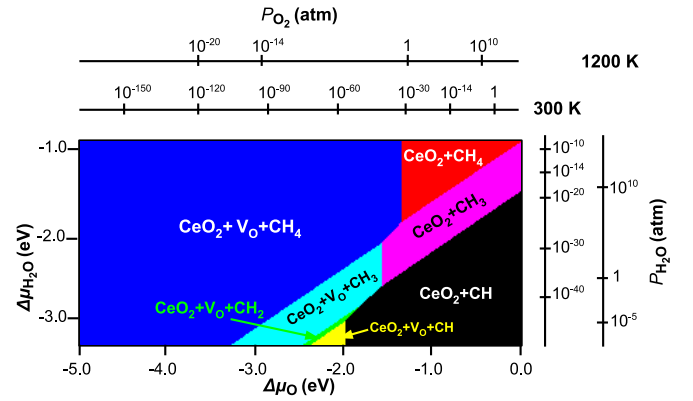


FIG. 6: Surface phase diagram of stable structures of $\text{CeO}_2(111)+\text{CH}_x$ in equilibrium with a humid environment, as a function of $\Delta\mu_{\text{O}}$ and $\Delta\mu_{\text{H}_2\text{O}}$ in the gas phase. The additional axes show the corresponding pressure scales at $T=300$ and 1200 K.

other areas CH_x fragments are stable, indicating the environmental conditions where CH_4 will dissociate on the $\text{CeO}_2(111)$ surface. As a general trend, for each fixed value of $\Delta\mu_{\text{O}_2}$ the partial pressure of the water plays an important role in the dehydrogenation process. In this case, the loss of one or more hydrogen atoms, and therefore the loss of one or more electrons by the methane molecule, is equivalent to an oxidation process.

Having defined the relative stability of each system, we now can consider under which conditions relevant transition phases occur. Fixing the chemical potential of water imposing a water-rich condition ($\Delta\mu_{\text{H}_2\text{O}} = -0.91$), for an atmospheric pressure $p=1$ atm, we find the surface to be reduced when the temperature is above $T \sim 1200$ K, while for $p=10^{-14}$, this value drops to $T \sim 500$ K, indicating that the pressure of the oxygen play a fundamental role in changing the critical temperature for surface reduction. Under atmospheric conditions, we can consider the partial pressure of the water vapor and oxygen to be around 1 atm. In this case the transition temperature between CeO_2+CH_4 and CeO_2+CH_3 is ~ 750 K, while between CeO_2+CH_3 and CeO_2+CH is $T \sim 1050$ K. This result suggests that a temperature above 750 K in the atmosphere is a sufficient condition for the partial oxidation of methane on the $\text{CeO}_2(111)$ surface which is in a good agreement with Haneda *et al.* who confirmed CeO_2 to show a catalytic activity for methane oxidation at 673 K.¹⁰ The difference could be due to the presence, supposedly small, of other facets rather than the more stable (111) in the specimen. As shown in Fig.6, there is a competing mechanism played by oxygen and water chemical potentials against methane dissociation. An increment of $\Delta\mu_{\text{H}_2\text{O}}$ would result in a higher critical temperature for CH_4 oxidation, while a change of $\Delta\mu_{\text{O}_2}$ would have the opposite effect. This result qualitatively confirms the effect of water on methane oxidation observed experimentally on several other materials.^{17,18}

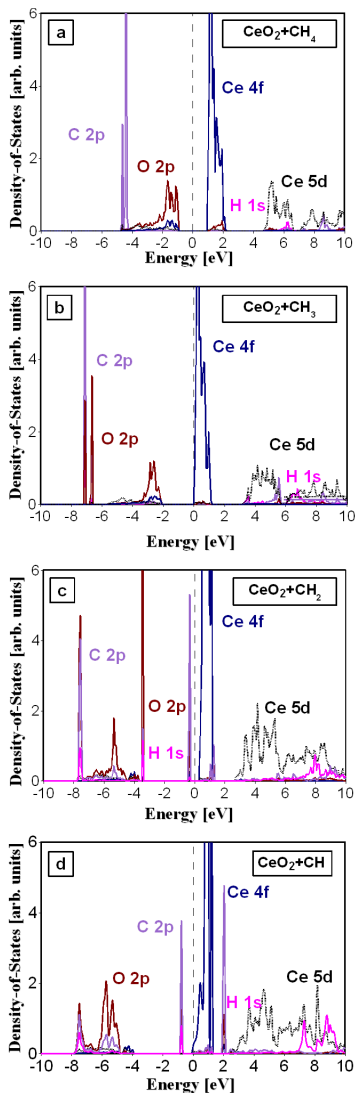


FIG. 7: Projected density-of-states of CH_x adsorbed on $\text{CeO}_2(111)$ surface. (a), (b), (c) and (d) represents the CH_4 , CH_3 , CH_2 and CH on the $\text{CeO}_2(111)$ surface. The black and the solid dark gray (blue) lines represent, respectively, the $5d$ and the $4f$ states of the cerium atoms, while the gray (red) line represents the $2p$ state of the oxygen atoms. The pale gray (magenta and purple) lines represent, respectively, the hydrogen $1s$ and carbon $2p$ of the CH_x fragment. The vertical dashed line represents the Fermi energy.

V. ELECTRONIC STRUCTURE

In this section, we analyze the electronic structures of the most stable surfaces identified in the previous section (Figs. 1, 2, 4 and 5).

Figure 7(a) shows the projected density-of-states (pDOS) for a stoichiometric surface with adsorbed methane molecule. There is no evidence of hybridization in the states of the carbon atom of the methane molecule and the nearest surface atoms. When focusing on the surface atoms, we observe that the $\text{CeO}_2(111)$ pDOS ex-

hibits a strong localization of the $\text{Ce-}4f$ band, typical of strongly correlated materials, centered at 1 eV, while the $\text{Ce-}5d$ states are delocalized in the range of 5 to 10 eV. The highest occupied band is mainly derived from the $2p$ state of oxygen, which has an overlap in energy with the $\text{Ce-}4f$ and $\text{Ce-}5d$ states in the range -5 eV to -1 eV. The $\text{C}_{\text{CH}_4}\text{-}2p$ peaks preserve their narrow profile, indicating a molecular-like behavior.

For the case of CH_3 chemisorbed on $\text{CeO}_2(111)$ (see Fig. 7(b)), the $\text{C}_{\text{CH}_3}\text{-}2p$ peaks shift toward lower energies by 2 eV. The $\text{O}_{\text{CeO}_2}\text{-}2p$ shows a splitting in two narrow peaks and there is an evident overlapping between $\text{C}_{\text{CH}_3}\text{-}2p$ and $\text{O}_{\text{CeO}_2}\text{-}2p$ at around -7 eV, indicating an evident surface-molecule interaction. This behavior is typical of atomic-like orbitals interacting with a narrow band, in this specific case the peak of $\text{O}_{\text{CeO}_2}\text{-}2p$.³⁰ In this case, the $\text{CeO}_2(111)$ surface shows a metallic behavior. However, the occupation of the $4f$ band is very low, and the energy of the surface can be considered indistinguishable to the semi-conductive surface.

When CH_2 adsorbs on the surface (see Fig. 7(c)), the hybridization of the orbitals is more evident. The $\text{O}_{\text{CeO}_2}\text{-}2p$ band shows a further shift to -6 eV and a broadening of the peak. There is also an evident overlapping of $\text{O}_{\text{CeO}_2}\text{-}2p$, $\text{O}_{\text{CH}_2}\text{-}2p$ and $\text{H}_{\text{CH}_2}\text{-}2p$ at around -8 eV and -4 eV, indicating a strong interaction.

When the fragment CH is adsorbed on the surface (see Fig. 7(d)), the narrow peak of the $\text{C}_{\text{CeO}_2}\text{-}2p$ exhibits a broadening, typical of atomic-like orbitals interacting with a broad band.³⁰ This feature suggests chemisorption of the adsorbate on the surface, that interacts with the band structure at surface level, consistent with the adsorption energy value previously shown. Also, in the adsorption of the CH fragment, the surface shows a metallic behavior. However, analogous considerations on the energy of the system can be done as in the case of the CH_3 adsorption.

VI. SUMMARY AND CONCLUSIONS

We performed DFT calculations in order to have an insight to the structure and energetics of CH_x adsorption on the stoichiometric and reduced $\text{CeO}_2(111)$ surface for a coverage of 0.25 ML. Our results show that, on the stoichiometric surface, the most stable structure is the one in which methane is adsorbed on Ce. However, the adsorption energy indicates a very weak interaction. Also, we found that surface oxygen vacancies do not increase the strength of the interaction, and that adsorption energies become stronger when methane is dehydrogenated. From the surface phase diagram, constructed by employing the *ab initio* constrained thermodynamics approach, we studied the relevant phase transitions. Fixing the chemical potential of water and imposing a water-rich condition, when the pressure of the atmosphere is $p=1$ atm, the reduced $\text{CeO}_2(111)$ surface is thermodynamically stable for a value of temperature is above $T\sim 1200$ K,

while for $p=10^{-14}$ this value drops to $T\sim 500$ K, indicating the fundamental role of the oxygen in determining the critical temperature for the reduction of the surface. Also, we estimated the sufficient conditions to obtain partial oxidation of the methane to be, considering the partial pressure of both water vapor and oxygen gas at 1 atm, 750 K, in good agreement with experimental results. A competing mechanism played by oxygen and water chemical potentials against methane dissociation was found, and while an increment of $\Delta\mu_{\text{H}_2\text{O}}$ would result in a higher critical temperature for CH_4 oxidation, a change of $\Delta\mu_{\text{O}_2}$ would have the opposite effect. This result qualitatively confirms the effect of water on methane

oxidation observed experimentally on several other material surfaces.

Acknowledgments

The authors gratefully acknowledge support from the Australian Research Council (ARC), the Australian National Computational Infrastructure (NCI) and the Australian Center for Advanced Computing and Communication (AC3). MF expresses his gratitude to Jason Gao and Irina Holca for proofreading the manuscript.

* Corresponding author.

E-mail: marco@gmail.com

- ¹ N. Long, Y. Yang, C. M. Thi, and M. N.V. Minhand Y. Cao and M. Nogami, *Nano Energy* **2**:5, 636 (2013).
- ² E. Kendrick and P. R. Slater, *Ann. Rep. Prog. Chem. A* **109**, 139 (2013).
- ³ P. Moussounda, M. Haroun, G. Rakotovelofy, and P. Légaré, *Surf. Sci.* **3697-3701**, 601 (2007).
- ⁴ B. Monnerat, L. Kiwi-Minsker, and A. Renken, *Chem. Eng. Sci.* **56**, 633 (2001).
- ⁵ L. Saraf, C. M. Wang, V. Shutthanandan, Y. Zhang, O. Marina, D. Baer, S. Thevuthasan, P. Nachimuthu, and D. Lindle, *J. Mat. Res.* **20**, 1295 (2005).
- ⁶ S. Kim and J. Maier, *J. Eur. Ceram. Soc.* **24**, 1919 (2004).
- ⁷ A. Trovarelli, *Catal. Rev. Sci.* **38**, 439 (1996).
- ⁸ A. Trovarelli, *Catal. Sci. Series* **2**, 407 (2002).
- ⁹ R. J. Farrauto, *Science* **337**, 659 (2012).
- ¹⁰ M. Haneda, T. Mizushima, and N. Kakuta, *J. Phys. Chem. B* **102**, 6579 (1998).
- ¹¹ N. Laosiripojana, S. Assabumrungrat, and S. Charo-irochkul, *The Joint International Conference on Sustainable Energy and Environment* (2004).
- ¹² D. Knapp and T. Ziegler, *J. Phys. Chem. C* **112**, 17311 (2008).
- ¹³ S. McIntosh and R. J. Gorte, *Chem. Rev.* **104**, 4845 (2004).
- ¹⁴ E. P. Murray, T. Tsai, and S. A. Barnett, *Nature* **400**, 649 (1999).
- ¹⁵ E. Odier, Y. Schuurman, and C. Mirodatos, *Cat. Today* **127**, 230 (2007).
- ¹⁶ S. Bharadwaj and L. Schmidt, *Fuel Proc. Tech.* **42**, 109 (1995).
- ¹⁷ C. F. Cullis and B. M. Willatt, *J. Catal.* **86**, 187 (1984).
- ¹⁸ F. H. Ribeiro, M. Chow, and R. A. Dallabetta, *J. Catal.* **146**, 537 (1994).
- ¹⁹ R. Kikuchi, S. Maeda, K. Sasaki, S. Wennerström, and K. Eguchi, *Appl. Cat. A* **232**, 23 (2002).
- ²⁰ A. D. Mayernick and M. J. Janik, *J. Phys. Chem. C* **112**, 14955 (2008).
- ²¹ C. Stampfl, *Catal. Today* **105**, 17 (2005).
- ²² K. Reuter and M. Scheffler, *Phys. Rev. B* **65**, 035406 (2002).
- ²³ K. Reuter and M. Scheffler, *Phys. Rev. B* **68**, 045407 (2003).
- ²⁴ C. Stampfl, M. V. Ganduglia-Pirovano, K. Reuter, and M. Scheffler, *Surf. Sci.* **500**, 368 (2002).
- ²⁵ J. P. Perdew, K. Burke, and M. Ernzerhof, *Phys. Rev. Lett* **77**, 3865 (1996).
- ²⁶ B. Delley, *J. Chem. Phys.* **92**, 508 (1990).
- ²⁷ B. Delley, *J. Chem. Phys.* **113**, 7756 (2000).
- ²⁸ M. Fronzi, A. Soon, B. Delley, E. Traversa, and C. Stampfl, *J. Chem. Phys.* **131**, 104701 (2009).
- ²⁹ M. Fronzi, S. Piccinin, B. Delley, E. Traversa, and C. Stampfl, *Phys. Chem. Chem. Phys.* **11**, 91889199 (2009).
- ³⁰ J. K. Nørskov, *Rep. Prog. Phys.* **53**, 1253 (1990).